Specific Heat of Single Crystal MgB_2: A Two-Band Superconductor with Two Different Anisotropies

F. Bouquet, Y. Wang, I. Sheikin, T. Plackowski, and A. Junod
DPMC, University of Geneva, 24 quai Ernest-Ansermet, 1211 Genève 4, Switzerland

S. Lee and S. Tajima
Superconductivity Research Laboratory, ISTEC, 1-10-13 Shinonome, Koto-ku, Tokyo 135-0062, Japan
(Received 4 July 2002; published 3 December 2002)

Heat-capacity measurements of a 39 μg MgB_2 single crystal in fields up to 14 T and below 3 K allow the determination of the low-temperature linear term of the specific heat, its field dependence, and its anisotropy. Our results are compatible with two-band superconductivity, the band carrying the smaller gap being isotropic, that carrying the larger gap having an anisotropy of $\sim$5. Three different upper critical fields are thus needed to describe the superconducting state of MgB_2.

DOI: 10.1103/PhysRevLett.89.257001 PACS numbers: 74.25.Bt, 74.25.Jb, 74.60.Ec, 74.70.Ad

Shortly after the discovery of 40-K superconductivity in MgB_2 [1], its nature was intensively studied. The isotope effect soon indicated phonon-mediated pairing [2]. However, MgB_2 cannot be considered as a classic conventional superconductor; indeed, several studies point to the existence of a gap much smaller than the expected BCS value: band-structure calculations [3,4], scanning tunneling microscopy (STM) [5,6], specific heat (C) [7–11], penetration depth [12], and various spectroscopic experiments [13–18]. The so-called "two-band" model [3,4], which considers two different s-wave superconducting gaps (a larger and a smaller gap, Δ_σ and Δ_π) on separate sheets of the Fermi surface (the σ and π bands, respectively), now seems widely accepted and explains most experimental results [19,20], with few exceptions [21]. The theory of two-band superconductivity was suggested soon after the development of the BCS theory [22], and some s-d metals have shown hints of this phenomenon, generally in the form of small deviations from BCS predictions, e.g., in C experiments [23]. In contrast, MgB_2 shows such clear signatures that it might serve as a textbook example. For instance, the electronic specific heat of MgB_2 shows an excess by an order of magnitude at $\sim T_c/5$ and presents an exponential dependence at low temperature (T), indicating the existence of a small gap on a large fraction ($\sim 50\%$) of the Fermi surface [7–11]. At low T, the effect of a small magnetic field (H) on the coefficient of the linear C term, $\gamma(H) \equiv \lim_{T\to 0} C(H)/T$, is dramatic. Classically, $\gamma(H)$, a thermodynamic probe of the electronic density of states at low energy, is expected to be linear in H up to H_{c2} [24]. However, for MgB_2 an extreme nonlinearity was observed, which was assigned to the existence of an additional, smaller gap [7–10].

The only specific heat experiment on single crystal reported so far was focused on the superconducting transition [25,26]. Such experiments are delicate since the mass of MgB_2 crystals is usually smaller than 100 μg, but are required to study the anisotropy. Previous studies showed that the anisotropy of superconducting properties depends on both field and temperature [27,28]. This puzzling behavior motivated the present study.

We measured the low-temperature specific heat of a MgB_2 single crystal with the field parallel and perpendicular to the boron planes. The results clearly show that the extreme nonlinearity of $\gamma(H)$, first observed in polycrystals [7–10], is an intrinsic property of MgB_2, related to the existence of two superconducting gaps. Moreover, these measurements reveal a dramatic variation of the effective anisotropy with the field, from 1 to $\sim$5. We interpret these results as a manifestation of the two-band nature of superconductivity in MgB_2, plus the dimensionality of the π band (isotropic) and σ band (anisotropic).

The single crystal of MgB_2 is similar to those described in Ref. [29]. Its mass, 39 μg, is small for a quantitative study of specific heat. For this purpose, we developed a miniaturized version of the relaxation calorimeter described in Ref. [7]. A commercial Cernox bare chip [30] was thinned down to 1 mg mass and used simultaneously as sample platform, heater, and thermometer. Two 10 μm phosphor-bronze wires soldered onto the chip acted as mechanical support, thermal links, and electrical leads. Only low-T studies were possible, since the heat capacity of the platform, essentially of phononic origin (sapphire), increases rapidly with T. We thus restrained our study to the range 2 to 3 K. Previous experiments have shown that this range of temperature lies sufficiently above the domain of possible parasitic magnetic contributions, but low enough ($\sim T_c/15$) to allow reliable determination of $\gamma(H)$ (see, e.g., Ref. [9]). Owing to the small value of C at these temperatures, the relaxation time was short (0.1–0.5 s), necessitating aperture times shorter than one power line cycle for the digitization of voltages. In order to suppress the 50 Hz noise, the signal was averaged over 50 to 200 relaxations. The field dependence of the addenda represents at most 13% of the

normal electronic linear term of the MgB_2 crystal and was calibrated by measuring a 196 μg Ag reference sample.

Figure 1 shows the specific heat for both orientations. It is impossible to compensate exactly for the small but unknown quantity of varnish used to attach the sample. Instead, in order to calculate $\gamma(H)$, we used the zero-field curve as a reference. It was shown on polycrystals that the electronic specific heat of MgB_2 is negligible in zero field in this temperature range [8–10]: the parallel shift of the C/T curves in Fig. 1 is thus a direct measurement of $\gamma(H)$. This shift was precisely determined by fitting each curve with a linear electronic term $\gamma(H)T$ plus a βT^3 lattice term, imposing the same β coefficient for all fields. The result for $\gamma(H)$ is plotted in Fig. 2 for both orientations. With the field perpendicular to the boron planes, $\gamma(H)$ saturates above 3–4 T, indicating that the sample has entered the normal state. This value is consistent with previous reports giving $\mu_0 H_{c2}^{(c)} \approx 3$ T for the upper-critical field along the c axis [25–27,31]. This also determines the normal electronic linear term $\gamma_n = 0.76 \pm 0.03$ mJ K^{-2} g-at.$^{-1}$, comparable with literature values [7–10]. The normal state is not fully established when the field is parallel to the (ab) planes, indicating that $H_{c2}^{(ab)}$ is higher than the maximum applied field of 14 T. An extrapolation suggests $\mu_0 H_{c2}^{(ab)} \approx 18$–22 T, in agreement with reported values [32]. Therefore, the anisotropy of the upper-critical field at $T \ll T_c$ is established in bulk.

The anisotropy of H_{c2} in MgB_2 has long been debated [32], but was finally assessed by experiments using clean single crystals [25–28,31]. Two kinds of anisotropy can be considered: the anisotropy of the superconducting gap and that of the Fermi surface. To model the former, some $\vec{k}$ dependence of the gap has to be assumed. Such an approach was attempted using a one-band model for MgB_2 [33]. The two-band model is an extreme case of such an anisotropy: depending on which Fermi sheet is considered, the superconducting gap may be either large or small. The effect of an anisotropic Fermi surface on superconducting properties can be modeled by renormalizing the isotropic results by a function of the ratio of the effective masses, a method that was successfully applied to cuprate superconductors [34]. Angst *et al.* used this approach for MgB_2 [27], but showed that the shape of the torque curves did not follow this simple one-band, anisotropic model over the whole range of field orientations.

From Fig. 2, it is clear that it is not possible to normalize the effect of the field by using a constant anisotropy factor. For $H \leq 0.5$ T, the values of $\gamma(H)$ are almost indistinguishable, irrespective of the field direction, showing the absence of anisotropy (see inset of Fig. 2). However, a field scaling factor of $\sim$5 is needed to superpose the $\gamma(H)$ curves just below saturation, i.e., near H_{c2}. An effective anisotropy Γ_{eff} can be defined as the scaling factor by which the field along the c axis must be multiplied in order to merge both $\gamma(H)$ curves. Figure 3 presents Γ_{eff} versus $H \parallel (ab)$. At low field, $\Gamma_{\text{eff}} \approx 1$, since the effect of H does not measurably depend on the orientation; Γ_{eff} rapidly increases with H and tends toward the anisotropy of H_{c2}, $\sim$5. Such an H-dependent anisotropy was also deduced from torque measurements [27]. The present analysis shows that the change of Γ_{eff} with H (and possibly with T) is an intrinsic property of MgB_2, having a bulk thermodynamic signature, even though the amplitude of this variation may depend on the physical quantity by which it is determined. We argue in the following that, to explain specific heat measurements, both kinds of anisotropy are required: the band dependence of the gap, *plus* a renormalization by the effective masses on the σ band.

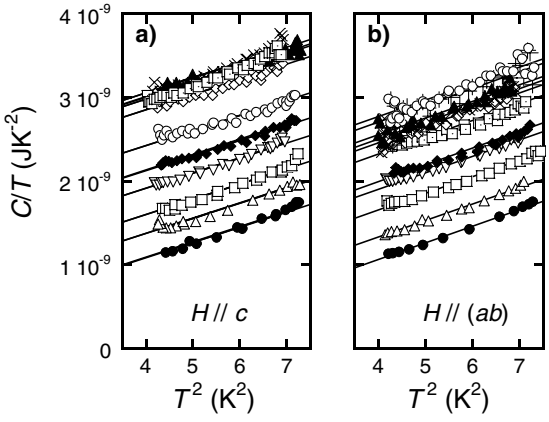

FIG. 1. Total specific heat, including that of addenda, for different magnetic fields (from bottom to top); (a) 0, 0.1, 0.2, 0.5, 1, 2, 3, 4, 6, and 10 T along the c axis; (b) 0, 0.1, 0.2, 0.5, 1, 3, 6, 8, 10, 12, and 14 T in the (ab) planes. The straight lines are linear fits with a common slope.

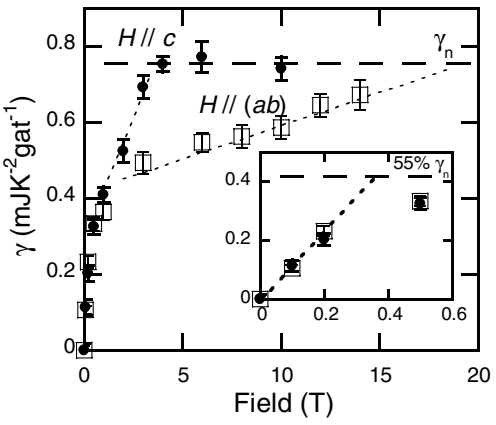

FIG. 2. Coefficient of the electronic linear term versus magnetic field applied parallel (□) or perpendicular (●) to the boron planes. The long-dashed line represents the normal state contribution. The short-dashed lines are guides for the eyes. Inset: expanded view of the low-field region; here the long-dashed line represents the partial normal-state contribution of the small-gapped band (see text and Fig. 4).

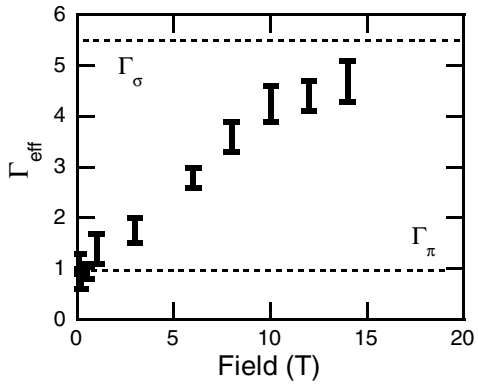

FIG. 3. Effective anisotropy, defined as the ratio of magnetic fields applied in the (ab) planes and along the c axis yielding the same γ value. Note that the choice of the abscissa is arbitrary: we chose $H \parallel (ab)$, but we could just as well plot it versus $H \parallel c$ or versus $\gamma(H)$.

Let us first focus on the shape of the $\gamma(H)$ curves. Similarly to previous data on polycrystals, $\gamma(H)$ increases sharply at low fields. The present data show that this effect does not depend on the orientation of the field and point to the existence of a large fraction of normal electrons in the mixed state already at very low H. In a typical s-wave, dirty type-II superconductor, $\gamma(H)$ mainly originates from the vortex cores and should be approximately proportional to H (i.e., the number of vortices). The strong nonlinearity of $\gamma(H)$ for MgB_2 is atypical: for $\mu_0 H = 1$ T, approximately half of γ_n is recovered, irrespective of the field direction. The effect is particularly striking for $H \parallel (ab)$: about 5% of $H_{c2}^{(ab)}$ drives $\sim$50% of the electrons into the normal state.

The peculiar shape of $\gamma(H)$ can be understood by considering the meaning of a vortex within a two-band model. Both bands supply the carriers and currents that define one vortex, and both bands contribute to the local density of states (LDOS) in one vortex core. Simulations [35] and STM studies [6] suggest that a core results from the superposition of two peaks in the LDOS with different diameters defined as usual by the coherence length ξ_σ or ξ_π associated with each band. The sharper peaks with diameter ξ_σ lead to a conventional core contribution for the σ band and overlap at H_{c2}. In contrast, the large coherence length of the π band gives rise to broad LDOS peaks, with a diameter much larger than $(\Phi_0/2\pi H_{c2})^{1/2}$. These giant cores, which have been observed by STM [6], contribute heavily to the total low-T DOS, as measured by $\gamma(H)$, until they start to overlap much below H_{c2}. At this point, the contribution of the π band to $\gamma(H)$ saturates. At higher fields, superconductivity in the π band is maintained up to H_{c2} by coupling to the σ band, but the variation of $\gamma(H)$ now comes from the σ-band contribution. The $\gamma(H)$ curves of Fig. 2 compare qualitatively well with these predictions. Note that the analysis of previous measurements on polycrystalline samples [7–10] was complicated by angular averaging of $\gamma(H \parallel c)$ and $\gamma(H \parallel ab)$, leading to a flattening above 8 T.

Within the present scheme, the data of Fig. 2 can be used to determine the anisotropy Γ_π and Γ_σ of each subsystem separately. The abnormally fast initial increase of $\gamma(H)$ at low H is attributed to the giant vortex cores associated with π-band carriers, and, as shown by the inset of Fig. 2, is isotropic; therefore, $\Gamma_\pi = 1$. On the other hand, the σ-band contribution is responsible for the anisotropy of H_{c2}, which we determined when describing Fig. 2; therefore, $\Gamma_\sigma \approx 6$. This is consistent with the 3D and quasi-2D character of the π and σ bands, respectively, found in band-structure calculations [4,19,20], and with the experimental determination by torque magnetometry at low T [27]. The *effective* anisotropy shown in Fig. 3 is a weighted average which depends on the relative contribution of each band to the condensate for a given H and T: it varies smoothly from Γ_π at low fields to Γ_σ at high fields.

Besides the anisotropy of each subsystem, we can attempt to determine the full shape of the unusual contribution of the π band, $\gamma^\pi(H)$. For this purpose, we assume that the σ-band contribution, $\gamma^\sigma(H)$, follows a classical behavior [24], increasing *linearly* from 0 to γ_n^σ as the field goes from 0 to $H_{c2}^{(c)}$or $H_{c2}^{(ab)}$, depending on the field orientation. The linear sections above 1 T in Fig. 2 correspond to this contribution of the σ band; their extrapolation to $H = 0$ points to the normal-state value γ_n^π of the π-band contribution ($\gamma_n^\pi + \gamma_n^\sigma = \gamma_n$). By subtracting $\gamma^\sigma(H)$ from $\gamma(H)$, we isolate $\gamma^\pi(H)$ (Fig. 4). The parameters $H_{c2}^{(c)}$, $H_{c2}^{(ab)}$, γ_n^π, and γ_n^σ are determined from Fig. 2. By requiring that the saturation value of $\gamma^\pi(H)$ is isotropic, we find that the parameters cannot depart by more than $\pm 15\%$ from the average fitted values $\mu_0 H_{c2}^{(c)} = 3.5$ T, $\mu_0 H_{c2}^{(ab)} = 19$ T, $\gamma_n^\pi = 0.42$ mJ K^{-2} g-at.$^{-1}$, and $\gamma_n^\sigma = 0.34$ mJ K^{-2} g-at.$^{-1}$. The $\gamma_n^\pi/\gamma_n^\sigma$ ratio $\approx 55/45 \approx 1$ is consistent with independent fits of the zero-field specific heat [11] and penetration depth [12] and with band-structure calculations [4,19,20]. Furthermore, $\gamma^\pi(H)$ appears to follow quantitatively numerical simulations [6,35]. This shows that a model consisting of two superfluids of nearly equal weight, having different gaps and different anisotropy, gives a consistent description of various properties of MgB_2.

The recent measurements of the thermal conductivity of single crystals by Sologubenko *et al.* [31] were interpreted in a similar way. At low fields, the heat conductivity increases sharply, for all field directions. As discussed for $\gamma(H)$, this is attributed to the contribution of normal 3D π-band carriers in the anomalously large vortex cores. At higher field, this effect saturates and the anisotropy rises, due to the increasing contribution of the quasi 2D σ band. A similar approach may explain not only why the anisotropy obtained from magnetic torque experiment changes with H and T, but also why a single-anisotropy model does not fit the angular dependence of H_{c2} [27,28]. We emphasize, however, that this view is simplified and phenomenological. A more elaborate description for the interaction between the two bands was

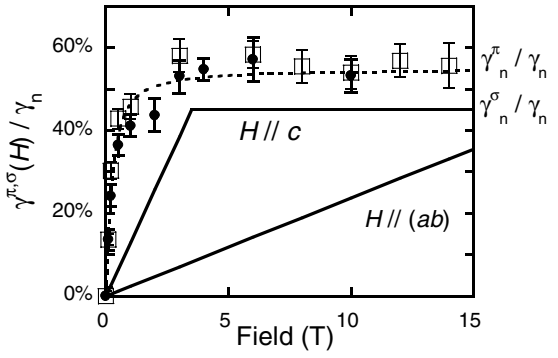

FIG. 4. Separation of both contributions to $\gamma(H)$: $\gamma^{\sigma}(H)$ (straight lines) and $\gamma^{\pi}(H)$ for the field applied along the c axis (●) and in the (ab) planes (□). The dashed line is a guide to the eyes for $\gamma^{\pi}(H)$.

proposed [36,37] for the anisotropy of penetration depth and its temperature dependence (which can be understood as a consequence of the rapid thermal depletion of the isotropic π-band condensate).

The phenomenological two-band model of Ref. [11] also uses two independent superfluids to explain the zero field C of MgB_2. Interband coupling was introduced by considering that the "virtual" T_c of the π band ($\Delta_\pi/1.76k_B \sim 13$ K) is brought up to that of the σ band; the peculiar features in C then originate from this superconductivity "above T_c." Here a somewhat similar situation arises: a virtual upper-critical field can be defined for the π band, $H^{\pi}_{c2} \sim (\Phi_0\Delta^2_\pi)/(\hbar^2 v^2_F)$ [38]; superconductivity persists up to $H^{(c)}_{c2}$ or $H^{(ab)}_{c2}$, depending on the field orientation, but above H^{π}_{c2} the overlap of huge vortex cores drives the majority of the π-band electrons normal (superconductivity "above H_{c2}"). Three characteristic fields are thus needed to describe the physics of MgB_2: the two upper-critical fields $H^{(c)}_{c2}$ and $H^{(ab)}_{c2}$ associated with the anisotropic σ band and a crossover field H^{π}_{c2} associated with the π band. We estimate the latter one by linearly extrapolating the low field $\gamma(H)$ to the partial normal state γ for this band ($\sim 0.55\gamma_n$), by analogy with classic superconductors. The inset of Fig. 2 shows this construction: we find $\mu_0 H^{\pi}_{c2} \approx 0.3$–$0.4$ T. These fields determine the values of the three coherence lengths of the system: for the anisotropic σ band $\xi^{(ab)}_{\sigma} \sim 10$ nm and $\xi^{(c)}_{\sigma} \sim 2$ nm; for the isotropic π band $\xi_{\pi} \sim 30$ nm. The latter value compares favorably with a direct measurement by STM giving 50 nm for the vortex-core diameter in the π band [6]. All *three* fields are needed to give a phenomenological description of the superconducting properties of MgB_2. Note that the ratio between $H^{(ab)}_{c2}$ and $H^{(c)}_{c2}$ is driven by Γ_σ, i.e., the anisotropy of the effective masses of the σ band, whereas the ratio between $H^{(c)}_{c2} \sim (\Phi_0\Delta^2_\sigma)/(\hbar^2 v^2_F)$ and H^{π}_{c2} is given by $\sim\Delta^2_\sigma/\Delta^2_\pi$, since the Fermi velocities are comparable on both bands. The experimental ratio $H^{(c)}_{c2}/H^{\pi}_{c2} \sim 10$ reported here agrees with various estimations of $\Delta_\sigma/\Delta_\pi \sim$ 3–3.5 [4,11–20].

Stimulating discussions with M. R. Eskildsen, T. Dahm, C. Berthod, and C. Marcenat are gratefully acknowledged. This work was supported by the Swiss National Science Foundation through the National Centre of Competence in Research "Materials with Novel Electronic Properties-MaNEP" and the New Energy and Industrial Technology Development Organization (NEDO).

[1] J. Nagamatsu *et al.*, Nature (London) **410**, 63 (2001).
[2] S. L. Bud'ko *et al.*, Phys. Rev. Lett. **86**, 1877 (2001).
[3] S.V. Shulga *et al.*, cond-mat/0103154.
[4] A. Y. Liu, I. I. Mazin, and J. Kortus, Phys. Rev. Lett. **87**, 087005 (2001).
[5] G. Rubio-Bollinger, H. Suderow, and S. Vieira, Phys. Rev. Lett. **86**, 5582 (2001).
[6] M. R. Eskildsen *et al.*, Phys. Rev. Lett. **89**, 187003 (2002).
[7] Y. Wang *et al.*, Physica (Amsterdam) **355C**, 179 (2001).
[8] F. Bouquet *et al.*, Phys. Rev. Lett. **87**, 047001 (2001).
[9] A. Junod *et al.*, in *Studies of High Temperature Superconductors*, edited by A.V. Narlikar (Nova Publishers, Commack, NY, 2002), Vol. 38, p. 179.
[10] H. D. Yang *et al.*, Phys. Rev. Lett. **87**, 167003 (2001).
[11] F. Bouquet *et al.*, Europhys. Lett. **56**, 856 (2001).
[12] F. Manzano *et al.*, Phys. Rev. Lett. **88**, 047002 (2002).
[13] X. K. Chen *et al.*, Phys. Rev. Lett. **87**, 157002 (2001).
[14] J.W. Quilty *et al.*, cond-mat/0206506.
[15] S. Tsuda *et al.*, Phys. Rev. Lett. **87**, 177006 (2001).
[16] F. Giubileo *et al.*, Phys. Rev. Lett. **87**, 177008 (2001).
[17] P. Szabó *et al.*, Phys. Rev. Lett. **87**, 137005 (2001).
[18] F. Laube *et al.*, Europhys. Lett. **56**, 296 (2001).
[19] A. A. Golubov *et al.*, J. Phys. Condens. Matter **14**, 1353 (2002).
[20] H. J. Choi *et al.*, Phys. Rev. B **66**, 020513 (2002); Nature (London) **418**, 758 (2002).
[21] H. Kotegawa *et al.*, Phys. Rev. B **66**, 064516 (2002); Phys. Rev. Lett. **87**, 127001 (2001).
[22] H. Suhl, B. T. Matthias, and L. R. Walker, Phys. Rev. Lett. **3**, 552 (1959).
[23] L. Y. L. Shen, N. M. Senozan, and N. E. Phillips, Phys. Rev. Lett. **14**, 1025 (1965).
[24] C. Caroli and J. Matricon, Phys. Kondens. Mater. **3**, 380 (1965).
[25] U. Welp *et al.*, cond-mat/0203337.
[26] L. Lyard *et al.*, cond-mat/0206231.
[27] M. Angst *et al.*, Phys. Rev. Lett. **88**, 167004 (2002).
[28] Y. Eltsev *et al.*, cond-mat/0202133.
[29] S. Lee *et al.*, J. Phys. Soc. Jpn. **70**, 2255 (2001).
[30] CX-1050-BR, see www.lakeshore.com.
[31] A.V. Sologubenko *et al.*, Phys. Rev. B **66**, 014504 (2002).
[32] C. Buzea and T. Yamashita, Supercond. Sci. Tech. **14**, R115 (2001).
[33] A. I. Posazhennikova, T. Dahm, and K. Maki, cond-mat/0204272.
[34] G. Blatter *et al.*, Rev. Mod. Phys. **66**, 1125 (1994).
[35] N. Nakai, M. Ichioka, and K. Machida, J. Phys. Soc. Jpn. **71**, 23 (2002).
[36] V. G. Kogan, Phys. Rev. B **66**, 020509 (2002).
[37] A. A. Golubov *et al.*, Phys. Rev. B **66**, 054524 (2002).
[38] S.V. Shulga and S.-L. Drechsler, cond-mat/0202172.